



Advanced MRI Findings in Medulloblastomas: Relationship to Genetic Subtypes, Histopathology, and Immunohistochemistry

Jonas Reis , Robert Stahl, Hanna Zimmermann, Viktoria Ruf, Niklas Thon, Mathias Kunz, Thomas Liebig, and Robert Forbrig 

From the Institute of Neuroradiology, University Hospital, LMU Munich, Munich, Germany (JR, RS, HZ, TL, RF); Department of Neuropathology, University Hospital, LMU Munich, Munich, Germany (VR); and Department of Neurosurgery, University Hospital, LMU Munich, Munich, Germany (NT, MK)

ABSTRACT

BACKGROUND AND PURPOSE: For diagnosis of medulloblastoma, the updated World Health Organization classification now demands for genetic typing, defining more precisely the tumor biology, therapy, and prognosis. We investigated potential associations between magnetic resonance imaging (MRI) parameters including apparent diffusion coefficient (ADC) and neuropathologic features of medulloblastoma, focusing on genetic subtypes.

METHODS: This study was a retrospective single-center analysis of 32 patients (eight females, median age = 9 years [range, 1-57], mean 12.6 ± 11.3) from 2012 to 2019. Genetic subtypes (wingless [WNT]; sonic hedgehog [SHH]; non-WNT/non-SHH), histopathology, immunohistochemistry (p53, Ki67), and the following MRI parameters were correlated: tumor volume, location (midline, pontocerebellar, and cerebellar hemisphere), edema, hydrocephalus, metastatic disease (presence/absence and each), contrast-enhancement (minor, moderate, and distinct), cysts (none, small, and large), hemorrhage (none, minor, and major), and ADC_{mean} . The ADC_{mean} was calculated using manually set regions of interest within the solid tumor. Statistics comprised univariate and multivariate testing.

RESULTS: Out of 32 tumors, three tumors were WNT activated (9.4%), 13 (40.6%) SHH activated, and 16 (50.0%) non-WNT/non-SHH. Hemispherical location ($n = 7/8$, $P = .003$) and presence of edema ($8/8$; $P < .001$, specificity 100%, positive predictive value 100%) were significantly associated with SHH activation. The combined parameter “no edema + no metastatic disease + cysts” significantly discriminated WNT-activated from SHH-activated medulloblastoma ($P = .036$). ADC_{mean} (10^{-6} mm²/s) was 484 for WNT-activated, 566 for SHH-activated, and 624 for non-WNT/non-SHH subtypes ($P = .080$). A significant negative correlation was found between ADC_{mean} and Ki67 ($r = -.364$, $P = .040$).

CONCLUSION: MRI analysis enabled noninvasive differentiation of SHH-activated medulloblastoma. ADC alone was not reliable for genetic characterization, but associated with tumor proliferation rate.

Keywords: Apparent diffusion coefficient, diffusion-weighted imaging, medulloblastoma, molecular groups, posterior fossa tumors.

Acceptance: Received October 28, 2020, and in revised form December 6, 2020. Accepted for publication December 24, 2020.

Correspondence: Address correspondence to Robert Forbrig, Institute of Neuroradiology, University Hospital, LMU Munich, Marchioninistrasse 15, 81377 Munich, Germany. E-mail: robert.forbrig@med.uni-muenchen.de.

Jonas Reis and Robert Stahl contributed equally to the work

Acknowledgements and Disclosure: The authors acknowledge that there was no external funding and no potential conflict of interest. Open access funding enabled and organized by Projekt DEAL.

J Neuroimaging 2021;31:306-316.

DOI: 10.1111/jon.12831

Introduction

Medulloblastomas, which are categorized as World Health Organization (WHO) grade IV, represent the most common malignant brain tumors of the childhood and commonly originate from the posterior fossa.¹ Medulloblastomas harbor highly variable individual prognoses. Conventional prognostic factors include patient age, tumor volume, extent of surgical tumor removal, any metastasis of tumor cells along the cerebrospinal fluid pathways, and the histopathological subtype.² Since the WHO classification of Central Nervous Tumors has been updated in 2016, diagnosis of medulloblastoma now demands for genetic typing additionally to histopathology,^{3,4} enabling a significantly improved prognostic evaluation. The worst prognosis is seen in sonic hedgehog (SHH)-activated tumors, partic-

ularly in those harboring an additional TP53 gene mutation, with a 5-year survival rate of about 40% despite aggressive therapy regimens.⁵ In here, novel therapeutic approaches such as targeted SHH inhibitors may be promising.⁶ Non-wingless (WNT)/non-SHH medulloblastomas bear an intermediate outcome and WNT-activated medulloblastomas (representing the genetic subtype with the lowest incidence of about 10%⁴) harbor the comparably best clinical courses with a survival rate of more than 90%.⁶⁻⁸ In addition to the genetic and histopathological classification of medulloblastomas, several immunohistochemical parameters (eg, pathological accumulation of p53 indicating the presence of a TP53 mutation, tumor proliferation index Ki67) enable further assessment of the tumors' activity and malignancy.^{9,10}

This is an open access article under the terms of the Creative Commons Attribution-NonCommercial-NoDerivs License, which permits use and distribution in any medium, provided the original work is properly cited, the use is non-commercial and no modifications or adaptations are made.

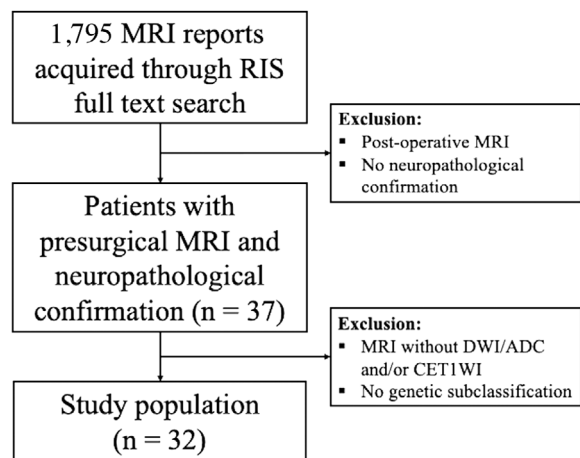


Fig 1. Flowchart of patient selection criteria.

ADC = apparent diffusion coefficient; CET1WI = contrast-enhanced T1-weighted imaging; DWI = diffusion-weighted imaging; n = number of patients; RIS = radiology information system.

Routine diagnostics of medulloblastoma comprise a magnetic resonance imaging (MRI) scan, yielding detailed conventional tumor parameters such as location, edema, hydrocephalus, metastatic disease, contrast enhancement, cysts, and hemorrhage. In this context, previous studies evaluated potential associations between conventional MRI parameters and histopathological and genetic subtypes of medulloblastoma, respectively, in the sense of a MRI biomarker assessment.^{11–15} The apparent diffusion coefficient (ADC) is a quantitative MRI parameter, representing a measure of water molecule diffusion. This parameter is independent of the field strength as it refers to the mean diffusivity that is rotationally invariant,^{16–18} and associated with tumor cell density.¹⁹ Several studies illustrated that ADC calculation within the neoplasm is valuable for both differential diagnosis of posterior fossa tumors^{20–24} and more accurate histopathological classification of medulloblastomas.¹³ However, systematic ADC data specifically considering the genetic subtypes and immunohistochemical features of medulloblastoma are clearly underrepresented in the literature.

Due to the paramount importance of adequate diagnostic and prognostic evaluation as a basis for tailored treatment regimens in commonly young patients with first diagnosis of medulloblastoma, this study particularly aimed at investigating potential associations between the ADC value and both genetic subtypes and immunohistochemistry (in addition to histopathology and conventional MRI parameters) for a better noninvasive characterization of these high-malignant brain tumors.

Methods

Patients

This retrospective single-center analysis included consecutive patients with first diagnosis of medulloblastoma who underwent brain MRI and subsequent open tumor resection at the University Hospital of the Ludwig-Maximilians-University Munich between January 2012 and October 2019. The flowchart in Figure 1 illustrates the patient selection criteria. In detail, patients were retrospectively identified via a full text query within the local radiology information system using the term “medulloblastoma.” The re-

sulting 1,795 reports were primarily filtered for presurgical MRI scans. Then, respective patient data were cross-checked for availability of neuropathological tumor parameters. Finally, presurgical MRI scans without diffusion-weighted imaging (DWI) and/or contrast-enhanced T1-weighted imaging (CET1WI) were excluded, resulting in a study population of 32 patients.

Neuropathological Examination

Diagnosis of medulloblastoma was neuropathologically confirmed for each patient at the department of neuropathology of our university medical center. All neoplasms were re-evaluated and categorized according the criteria defined by the revised WHO Classification of Tumors of the Central Nervous System 2016 considering current recommendations.^{3,9} In detail, the following medulloblastoma parameters were assessed:

- Genetic subtype: WNT, SHH, and non-WNT/non-SHH;
- Histopathological subtype: classic, desmoplastic, extensive nodularity, and large-cell/anaplastic;
- Immunohistochemistry: presence/absence of a TP53 mutation and tumor proliferation index Ki67.

MRI Protocol

MRI was conducted in a single center using two scanners with different field strengths (1.5 Tesla, Aera, Siemens Healthineers and 3 Tesla, Signa, General Electric). The presurgical MRI protocol of the brain routinely comprised the following sequences: axial and/or coronal spin-echo T2-weighted imaging (T2WI) with a slice thickness of 3–5 mm, axial and/or coronal T2-weighted fluid-attenuated inversion recovery (FLAIR) with a slice thickness of 5 mm, axial gradient-echo noncontrast and CET1WI with coronal and sagittal reconstructions and a slice thickness of 1 mm, and DWI. The following DWI parameters were routinely applied: sequence type, spin-echo echo planar imaging; repetition time ms/echo time ms, 5,700/91 (1.5 Tesla) and 9,200/91 (3 Tesla); slice thickness, 5 mm with no gap; matrix, 130 × 130 (1.5 Tesla) and 180 × 180 (3 Tesla); and field of view, 23 cm². Diffusion data were obtained for three orthogonal axes along the static magnetic field. The respective ADC maps were automatically generated from b0 and b1000 data. Furthermore, MRI of the whole spine was performed in each patient in combination with the cranial MRI either before or within 72 hours after tumor resection²⁵ to detect/rule out spinal seeding, including spin-echo T2WI and CET1WI sequences, each in axial (slice thickness 4 mm) and sagittal planes (slice thickness 3 mm).

MRI Analysis

Regarding MRI analysis, two neuroradiologists with 4 (J.R.) and 10 (R.F.) years of experience in diagnostic neuroradiology who were blinded to neuropathological, and clinical data evaluated the following conventional tumor parameters in consensus:

- Volume (cm³), computed with a dedicated open-source DICOM software (Horos 3.3.6 for MAC, www.horosproject.org) using manually set regions of interest (ROIs) that define the solid tumor margins in T2WI and/or CET1WI sequences;
- Location: midline/cerebellar vermis, cerebellopontine angle (CPA), cerebellar hemisphere (according to Perreault and colleagues¹²);

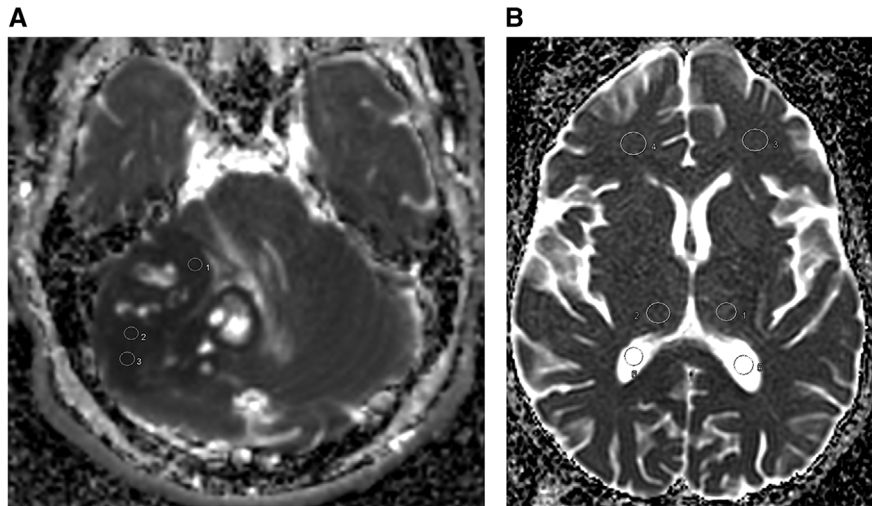


Fig 2. Example apparent diffusion coefficient (ADC) measurement of medulloblastoma (A). Three regions of interest (ROI) were manually placed within the solid tumor components, yielding mean ADC (10^{-6} mm²/s) values of 496 ± 18 standard deviation (SD) (ROI 1), 429 ± 17 SD (ROI 2), and 414 ± 17 SD (ROI 3). Control measurements (B) yielded mean ADC (10^{-6} mm²/s) values of 856 ± 90 SD (ROI 1) and 836 ± 73 SD (ROI 2) for the thalamus, 853 ± 51 SD (ROI 3) and 875 ± 57 SD (ROI 4) for white matter as well as 3141 ± 209 SD (ROI 5) and 3243 ± 204 SD (ROI 6) for pure CSF. In each patient, measurements were conducted for several subsequent slices and averaged.

- Edema: presence, absence (using T2WI/FLAIR and DWI);
- Hydrocephalus, defined as widening of the lateral ventricles and third ventricle due to infratentorial mass effect with subsequent transependymal diapedesis of cerebrospinal fluid;
- Metastatic disease, defined as macroscopically visible subependymal, ventricular, or meningeal nodules or masses in cranial and/or spinal MRI (Chang M-stage ≥ 2)²⁶;
- Contrast enhancement: minor, moderate, distinct (based on Keil and colleagues¹¹);
- Cysts: none, small ≤ 1 cm, large > 1 cm (according to Yeom and colleagues¹³);
- Hemorrhage: none, minor (without mass effect), major (with mass effect).

Quantitative ADC Analysis

A neuroradiologist (J.R.) with 4 years of experience in diagnostic neuroradiology who was blinded to neuropathological and clinical data performed ADC measurements in each presurgical MRI, using a dedicated picture archiving and communication system (syngo Imaging, Siemens Healthineers). In detail, ROIs with a size of 30-100 mm² were manually placed within the solid tumor components as previously described,^{22,27} carefully avoiding inhomogeneous regions such as cysts or hemorrhage. To decrease the amount of discordant values, measurements were carried out thrice for each slice in each patient, yielding at least six to nine ROIs. An example measurement is illustrated in Figure 2A. Furthermore, ROIs were manually placed within healthy appearing gray matter (thalamus) and white matter (frontal lobe) as well as within the lateral ventricles (Fig 2B). For calculation of the ADC_{mean}, results of ROI calculation were averaged. A senior neuroradiologist (R.F.) confirmed the correct ROI placement.

Statistics

Discrete and continuous data were initially assessed for normality using the Shapiro-Wilk test and by visual inspection of their histograms. Based on these results, we used one-way analysis of variance (ANOVA) for the tumor volume and ADC to test

for equality of mean values in each data group. When statistically significant differences occurred, single posttest comparisons were performed by using pairwise *t*-tests. Intergroup differences in the Ki67 were tested with the Kruskal-Wallis test. The difference in tumor volume between midline/cerebellar vermis and elsewhere located lesions was conducted with a two-tailed *t*-test. Furthermore, *t*-tests were used to assess differences in the mean ADC values of the tumor between the magnetic field strengths as well as in the mean ADC values between subtypes with presence and absence of p53 accumulation on immunohistochemistry, edema, hydrocephalus, and metastatic disease. Mean ADC values of the tumor with the Ki67 indices as well as mean ADC values of the healthy appearing control regions with age were correlated by using the Spearman rank correlation test. Differences in mean ADC values of the corresponding control regions between the different field strengths of the MRI scanners were assessed with the Mann-Whitney *U* test. Normally distributed variables are provided as mean \pm standard deviation (range). Variables that do not follow normal distribution are shown as median (25%; 75% interquartile range). For binary (eg, histopathological subtype) or categorical (eg, conventional MRI parameters such as presence and size of cysts) variables, contingency tables were created. Fisher exact tests were used to test if the variable was independently distributed within the genetic entities. When statistically significant differences occurred, several single post hoc 2×2 Fisher exact tests were calculated. This subsequent analysis included pairwise comparisons of all tumor subtypes as well as the comparison of each tumor subtype with the combined data of the other two entities. For each variable, the sensitivity, specificity, positive predictive value (PPV), negative predictive value (NPV), and area under the receiver operating characteristic curve (AUC) including 95% confidence intervals (CIs) were calculated. Analysis was performed using R (version 3.6.1/R Core Team (2019)/<https://www.R-project.org/>) on R-Studio Version 1.2.5001 and the SPSS statistical package (IBM Corp. Released 2017. IBM SPSS Statistics for Windows, Version 25.0. Armonk,

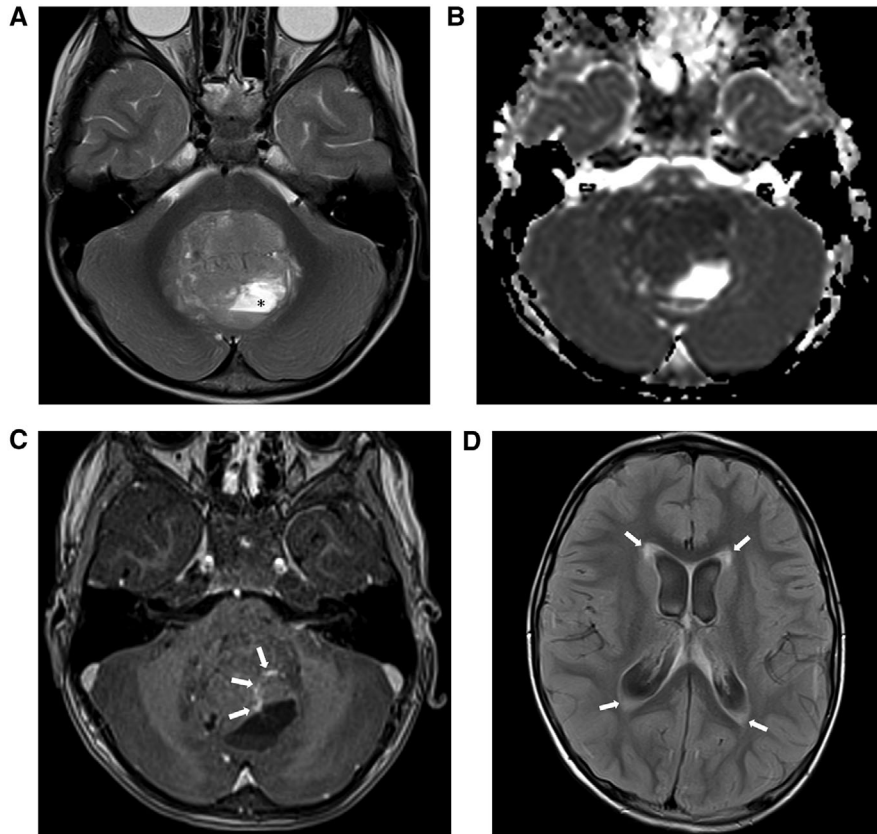


Fig 3. Wingless-activated medulloblastoma (patient #1): Neuropathological characteristics were a classic subtype in histopathology, a TP53 wild type, and a Ki67 of 40%. T2-weighted imaging showed a midline/cerebellar vermian tumor location with a volume of 48.7 cm³ and a large intratumoral cyst harboring a fluid-fluid level caused by minor hemorrhage (black asterisk, A). Peritumoral edema was absent. Apparent diffusion coefficient (ADC) map with a calculated mean ADC (10⁻⁶ mm²/s) of 606 ± 34 standard deviation (B). Contrast-enhanced T1-weighted imaging showed only circumscribed contrast-enhancing intratumoral components (white bold arrows, C). T2-weighted fluid-attenuated inversion recovery imaging yielded signs of cerebrospinal fluid diapedesis (white bold arrows, D). No metastatic disease was found.

NY: IBM Corp.). *P*-values were adjusted by using Bonferroni correction for multiple comparisons. A level of significance of $\alpha = 0.05$ was used throughout the study.

Results

Baseline characteristics, genetic and histopathological classification, immunohistochemistry as well as MRI parameters of the study population are illustrated in Table 1. Eight of 32 patients (25%) were female. The median and mean patient age at diagnosis was 9 years (range, 1-57 years) and 12.6 ± 11.3 years, respectively, with 26 of 32 (81%) pediatric and six of 32 (19%) adult medulloblastomas (cutoff, 21 years¹¹).

Neuropathology

Results of neuropathologic correlations with genetic subtypes are presented in Table 2. Out of 32 tumors, three (9.4%) tumors showed a WNT activation, 13 (40.6%) were SHH activated including all six adult cases, and 16 (50.0%) were classified as non-WNT/non-SHH (group 3 or 4). Out of 32 tumors, eighteen (56.25%) were categorized as classic, eight (25%) as desmoplastic, two (6.25%) as extensive nodular, and four (12.5%) as large cell/anaplastic. Absence of a classic subtype was significantly associated with SHH pathway activation ($P < .0001$; sensitivity = 92.3%; specificity = 89.5%; PPV = 85.7%; NPV = 94.4%; AUC = 0.909). In contrast, all right tumors exhibiting a desmo-

plastic subtype exclusively belonged to the 13 SHH-activated medulloblastomas ($P < .0001$; sensitivity = 61.5%; specificity = 100%; PPV = 100%; NPV = 79.2%; AUC = 0.808). Strong nuclear expression of p53 on immunohistochemistry reflecting mutations of the TP53 gene was seen in 3 of 32 (9.4%) patients, all suffering from SHH-activated tumors ($P = .055$). No significant association was found between tumor cell proliferation (Ki67) and the genetic profile ($P = .176$).

MRI Analysis

Table 2 provides detailed information of correlations between MRI parameters and genetic subtypes. Figures 3–5 illustrate three example patients with WNT-activated (patient #1, Fig 3A-D), SHH-activated (patient #15, Fig 4A-D), and non-WNT/non-SHH medulloblastoma (patient #29, Fig 5A-F).

The mean tumor volume was 30.1 cm³ (range, 4.4-63.2 cm³) and did not differ between the genetic subtypes ($P = .157$). Univariate analysis revealed a significant difference of tumor location between the genetic subtypes ($P = .005$). In detail, non-WNT/non-SHH medulloblastomas were significantly more frequently located in the midline/cerebellar vermian (14/16, 87.5%) when compared to SHH-activated tumors (4/13, 30.8%; $P = .003$; sensitivity = 87.5%; specificity = 69.2%; PPV = 77.8%; NPV = 81.8%; AUC = 0.784). Hemispherically located medulloblastomas showed activation of the SHH pathway in the

Table 1. Baseline Characteristics, Genetic and Histopathological Subtype, Immunohistochemistry as well as MRI Parameters of 32 Patients with Medulloblastoma

#	Age Sex	Genetic Subtype	Histopathologic Subtype	TP53 Mutation	Ki67 (%)	Volume (cm ³)	Location	Edema	Hydrocephalus	MD	CE	Cysts	Hemorrhage	ADC _{mean} ± SD (10 ⁻⁶ mm ² /s)
1	3M	WNT	Classic	No	40	48.7	Midline	No	Yes	No	Minor	Large	Minor	606 ± 34
2	9M	WNT	Classic	No	70	61.3	Midline	No	Yes	No	Moderate	Large	No	269 ± 48
3	19F	WNT	Classic	No	40	6.2	CPA	No	No	No	Moderate	Small	No	577 ± 38
4	7M	SHH	Classic	No	15	18.9	Midline	No	Yes	No	Minor	Small	Minor	682 ± 33
5	5F	SHH	Large cell/anaplastic	Yes	40	24.0	CPA	No	Yes	Yes	Minor	No	Minor	580 ± 14
6	19M	SHH	Desmoplastic	No	25	21.2	Hemispheric	Yes	No	No	Minor	Large	Minor	448 ± 70 [#]
7	3M	SHH	Desmoplastic	No	30	22.3	Hemispheric	Yes	No	Yes	Minor	No	No	593 ± 38
8	22M	SHH	Desmoplastic	No	20	29.4	Hemispheric	No	Yes	Yes	Minor	Small	No	570 ± 104
9	22M	SHH	Desmoplastic	No	30	17.6	CPA	No	No	No	Moderate	Small	No	562 ± 53
10	18F	SHH	Desmoplastic*	Yes	60	15.7	Hemispheric	Yes	No	No	Moderate	Large	No	491 ± 77 [#]
11	30F	SHH	Desmoplastic	No	25	14.2	Hemispheric	No	Yes	No	Moderate	Small	No	523 ± 39 [#]
12	57M	SHH	Desmoplastic	No	70	11.0	Hemispheric	Yes	No	Yes	Moderate	Small	No	430 ± 42
13	2M	SHH	Extensive nodularity	No	20	16.4	Midline	Yes	Yes	Yes	Distinct	No	No	665 ± 92
14	1M	SHH	Extensive nodularity	No	50	39.6	Midline	Yes	Yes	No	Distinct	Small	No	681 ± 30
15	29M	SHH	Desmoplastic	No	75	55.0	Hemispheric	Yes	No	No	Distinct	Small	No	451 ± 21
16	23M	SHH	Large cell/anaplastic	Yes	40	27.4	Midline	Yes	No	Yes	Minor	Small	Minor	650 ± 24
17	16M	Non-WNT/Non-SHH	Classic	No	20	32.5	Midline	No	Yes	Yes	Minor	Small	Minor	453 ± 61 [#]
18	8M	Non-WNT/Non-SHH	Classic	No	60	36.3	Midline	No	Yes	No	Minor	Small	No	505 ± 43
19	10M	Non-WNT/Non-SHH	Classic	No	25	30.9	Midline	No	Yes	No	Minor	Large	No	546 ± 87
20	9M	Non-WNT/Non-SHH	Classic	No	30	63.2	Midline	No	Yes	No	Minor	Large	No	683 ± 73
21	5F	Non-WNT/Non-SHH	Classic	No	30	36.8	Midline	No	Yes	No	Minor	Small	Minor	674 ± 41
22	12M	Non-WNT/Non-SHH	Classic	No	20	39.8	Midline	No	Yes	No	Minor	Small	No	716 ± 49
23	8F	Non-WNT/Non-SHH	Classic	No	60	36.4	Midline	No	Yes	No	Minor	Large	No	701 ± 65
24	9M	Non-WNT/Non-SHH	Large cell/anaplastic	No	30	4.4	Hemispheric	No	No	Yes	Minor	Small	No	555 ± 74 [#]
25	8M	Non-WNT/Non-SHH	Classic	No	20	38.8	Midline	No	Yes	Yes	Moderate	Large	No	631 ± 78
26	15M	Non-WNT/Non-SHH	Classic	No	25	48.1	Midline	No	Yes	No	Moderate	Large	Minor	653 ± 61
27	4M	Non-WNT/Non-SHH	Large cell/anaplastic	No	30	16.5	Midline	No	Yes	Yes	Moderate	No	No	535 ± 34
28	7F	Non-WNT/Non-SHH	Classic	No	25	20.0	Midline	No	Yes	Yes	Moderate	No	No	715 ± 29
29	8M	Non-WNT/Non-SHH	Classic	No	40	17.9	Midline	No	No	Yes	Moderate	Small	No	510 ± 46
30	5M	Non-WNT/Non-SHH	Classic	No	40	28.4	Midline	No	Yes	Yes	Moderate	Small	Minor	585 ± 31
31	7F	Non-WNT/Non-SHH	Classic	No	25	35.6	CPA	No	Yes	Yes	Moderate	Small	No	827 ± 38
32	2M	Non-WNT/Non-SHH	Classic	No	30	48.7	Midline	No	Yes	No	Distinct	Large	No	696 ± 36

Apparent diffusion coefficient values were retrieved from 1.5 Tesla (n = 27) and 3 Tesla (#, n = 5) examinations.

*Desmoplastic medulloblastoma with anaplastic features in histopathology.

ADC = apparent diffusion coefficient; CE = contrast enhancement; CPA = cerebellopontine angle; F = female; M = male; MD = metastatic disease; SD = standard deviation; SHH = sonic hedgehog pathway activation = WNT, wingless pathway activation.

Table 2. Genetic Subtype Analysis of Histopathology and Immunohistochemistry as well as MRI Parameters in 32 Patients with Medulloblastoma

Genetic subtype	WNT (n = 3)	SHH (n = 13)	Non-WNT/Non-SHH (n = 16)	P-value
Histopathologic subtype				
Classic	3	1	14	Fisher exact: $P < .001$
Desmoplastic	0	8	0	Fisher exact: $P < .001$
Extensive nodularity	0	2	0	Fisher exact: $P = .192$
Large cell/anaplastic	0	2	2	Fisher exact: $P = 1.000$
Immunohistochemistry				
TP53 mutation (n)	0	4	0	Fisher exact: $P = .055$
Ki67 (%), median (25%; 75% percentile)	40 (40; 40)	30 (22.5; 55)	30 (25; 37.5)	Kruskal Wallis: $P = .176$
MRI analysis				
Volume (cm ³), mean (range)	38.7 (6.2-61.3)	24.0 (11.0-55.0)	33.4 (4.4-63.2)	ANOVA: $P = .157$
Location (midline/CPA/hemispheric)	2/1/0	4/2/7	14/1/1	Fisher exact: $P = .005$
Edema (n)	0	8	0	Fisher exact: $P < .001$
Hydrocephalus (n)	2	6	14	Fisher exact: $P = .067$
Metastatic disease (n)	0	6	8	Fisher exact: $P = .343$
Contrast enhancement (minor/moderate/distinct)	1/2/0	6/4/3	8/7/1	Fisher exact: $P = .669$
Cysts (none/small/large)	0/1/2	3/8/2	2/8/6	Fisher exact: $P = .423$
Hemorrhage (none, minor, major)	2/1/0	9/4/0	12/4/0	Fisher exact: $P = 1.000$
ADC _{mean} (10 ⁻⁶ mm ² /s) ± SD (95% KI)	484 ± 187 (200-948)	566 ± 88 (507-625)	624 ± 101 (570-678)	ANOVA: $P = .080$
Correlation	$r = -.364$	Spearman: $P = .040$		
ADC _{mean} /Ki67 (n = 32)				

ADC = apparent diffusion coefficient; CPA = cerebellopontine angle; n = number of patients; SHH = sonic hedgehog pathway activation; WNT = wingless pathway activation.

majority of cases (7/8, 87.5%; $P = .003$; sensitivity = 53.8%; specificity = 94.7%; PPV = 87.5%; NPV = 75.0%; AUC = 0.743). The location of WNT-activated tumors ($n = 3$; two midline/cerebellar vermis and one CPA) was not significantly different in comparison to the non-WNT/non-SHH subtypes ($P > .05$).

Peritumoral edema was noted in eight patients, all presenting with SHH activation ($n = 8/13$, 61.5%). Consequently, presence of edema discriminated SHH-activated medulloblastoma significantly from the other genetic subtypes with a specificity and PPV of each 100% ($P < .0001$; sensitivity = 61.5%; NPV = 79.2%; AUC = 0.808). No significant associations were found between the genetic subtypes and the MRI parameters hydrocephalus, metastatic disease, contrast enhancement, cyst formations, and hemorrhage ($P > .05$, each). Hydrocephalus occurred significantly more frequently if the tumor was located in the midline/cerebellar vermis when compared to a hemispheric or CPA location ($n = 18/20$, 90.0% vs. 4/12, 33.3%; Fisher exact test: $P = .002$). Of note, midline/cerebellar vermis medulloblastomas also had a significantly larger volume (mean 35.3 vs. 21.4 cm³; t -test: $P = .010$).

Regarding multivariate analysis, the combined parameter “presence of edema + presence of metastatic disease” was only documented in SHH-activated tumors (4/13, 30.8%). Thus, it discriminated this subtype significantly from the other genetic subtypes with a specificity and PPV of each 100% ($P = .020$; sensitivity = 30.8%; NPV = 67.9%; AUC = 0.654). Furthermore, the combined parameter “absence of edema + absence of metastatic disease + presence of cysts” differentiated WNT-activated medulloblastoma significantly from the SHH-activated subtype with a sensitivity and NPV of each 100% ($P = .036$; specificity = 76.9%; PPV = 50.0%; AUC = 0.885).

Quantitative ADC Analysis

Results of quantitative ADC analysis are illustrated in Table 2 and Figure 6. Overall, the calculated ADC_{mean} (10⁻⁶ mm²/s) within the solid tumor was 586 ± 111 (546-626) and significantly different between the applied field strengths (1.5 Tesla, $n = 27/32$: 603 ± 111 [559-647]; 3 Tesla, $n = 5/32$: 494 ± 46 [437-551]; $P = .040$). In detail, the calculated ADC_{mean} (10⁻⁶ mm²/s) was 484 ± 187 (200-948) for WNT-activated, 566 ± 88 (507-625) for SHH-activated, and 624 ± 101 (570-678) for non-WNT/non-SHH medulloblastoma (Table 2 and Fig 6A; $P = .080$). Regarding histopathology, the respective ADC_{mean} (10⁻⁶ mm²/s) was 613 ± 126 (550-675) for classic, 509 ± 63 (456-561) for desmoplastic, 673 ± 11 (571-775) for extensive nodular, and 580 ± 50 (500-660) for large cell/anaplastic medulloblastoma, yielding a significant difference between the desmoplastic and extensive nodular subtype (Fig 6B; $P < .0001$).

A significant negative correlation was found between ADC_{mean} and the proliferation parameter Ki67 (Table 2 and Fig 6C; $r = -.364$, $P = .040$, $n = 32$). The ADC_{mean} was neither significantly different regarding TP53 ($P = .412$) nor the conventional MRI parameters (location: $P = .161$; edema: $P = .307$; contrast enhancement: $P = .560$; cysts: $P = .769$; hemorrhage: $P = .852$; hydrocephalus: $P = .083$; metastatic disease: $P = .777$).

Control ADC measurements within the gray and white matter as well as CSF yielded no significant differences when comparing magnetic field strengths and no significant correlations with patient age (Fig 7). In detail, median ADC (10⁻⁶ mm²/s) values (25%; 75% quartile) were 786 (733; 823) at 1.5 Tesla versus 818 (683; 888) at 3 Tesla within the thalamus ($P = .697$), 801 (717; 852) at 1.5 Tesla versus 790 (701; 847) at 3 Tesla within white matter ($P = .736$), and 3152 (3008; 3322) at 1.5 Tesla

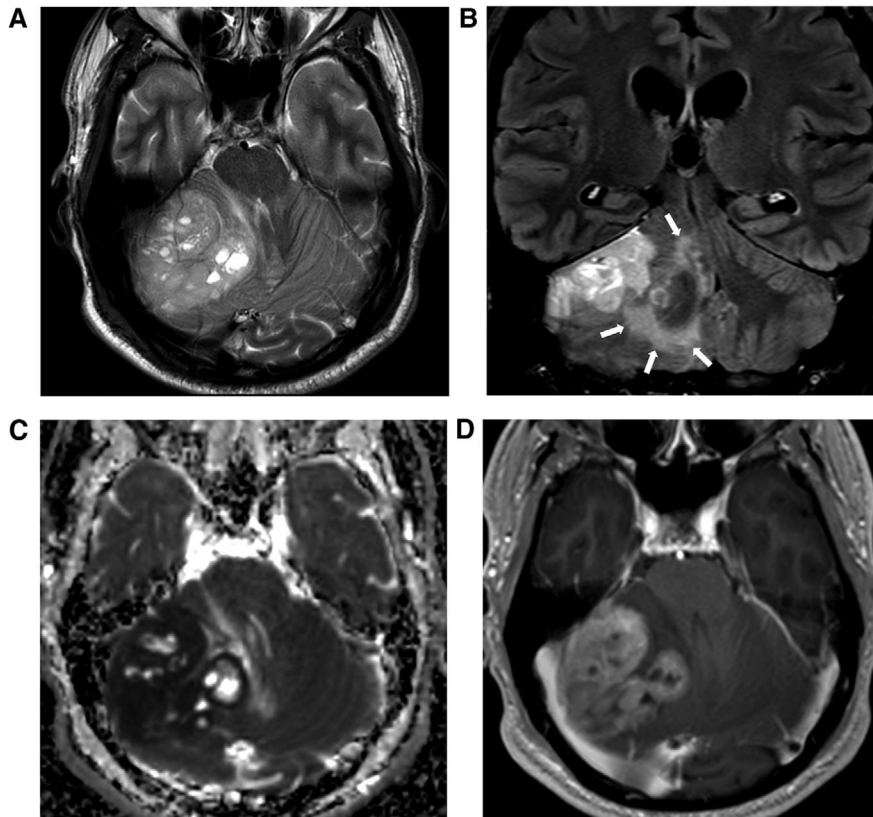


Fig 4. Sonic hedgehog-activated medulloblastoma (patient #15): Neuropathological characteristics were a desmoplastic subtype in histopathology, a TP53 wild type, and a Ki67 of 75%. T2-weighted imaging showed a hemispherical tumor location with a volume of 55.0 cm³ and several small intratumoral cysts but no hemorrhage (A). T2-weighted fluid-attenuated inversion recovery imaging showed peritumoral edema (white bold arrows, B) and absence of cerebrospinal fluid diapedesis. Apparent diffusion coefficient (ADC) map with a calculated mean ADC (10⁻⁶ mm²/s) of 451 ± 21 standard deviation (C). Contrast-enhanced T1-weighted imaging showed distinct contrast enhancement of the solid tumor (D). No metastatic disease was documented.

versus 3061 (2952; 3115) at 3 Tesla within the lateral ventricle ($P = .421$).

Discussion

In the present study, we correlated several MRI parameters (including quantitative ADC) with neuropathologic features of medulloblastoma, focusing on the genetic subtypes according to the updated 2016 WHO classification of Central Nervous Tumors. Numerous conventional MRI parameters (ie, hemispheric location, peritumoral edema, and metastatic disease) were identified that specifically allowed for the noninvasive diagnosis of an aggressive SHH pathway activation, possibly yielding a quicker (presurgical) initiation of proper therapy regimens in patients suffering from this specific genetic subtype. Moreover, we calculated mean ADC values within the solid tumor components that showed no significant association with the genetic but rather the histopathologic subtypes of medulloblastoma; the ADC values were also associated with the tumor's proliferation rate.

Several studies investigated conventional MRI parameters in medulloblastoma patients in order to detect potential cross-sectional biomarkers.¹¹⁻¹⁵ Similar to other authors,^{12,14,15} in the present study seven of eight (87.5%) hemispherically located tumors showed a SHH pathway activation, which was statisti-

cally significant when compared to the other genetic subtypes. Thus, we conclude that a tumor location within the cerebellar hemisphere is typical for SHH-activated medulloblastoma. However, we agree with Teo and colleagues¹⁵ that this subtype may also be located in the CPA or within the midline/cerebellar vermis (this study: $n = 6/13$ SHH-activated tumors). In here, most common midline neoplasms were non-WNT/non-SHH medulloblastomas ($n = 14/20$), resulting in a significant difference when compared to the SHH-activated subtype alone. These results confirm findings of other studies.^{12,14,15} However, our data illustrate that—similar to the findings of Patay and colleagues²⁸—the WNT-subtype is also frequently located in the midline (two of 3 patients, 67%), disabling further differentiation between WNT-activated and non-WNT/non-SHH medulloblastoma solely based on anatomic distribution. Of note, Perreault and colleagues¹² located WNT-activated tumors more commonly in the CPA (75%).

In this study, the strongest MRI parameter was the presence of peritumoral edema, which was documented in eight of 32 (25%) patients with first diagnosis of medulloblastoma. Each of these eight tumors showed activation of the SHH pathway, yielding a specificity and positive predictive value of 100%, each. A similar tendency was reported by Keil and colleagues,¹¹ who calculated a significantly larger edema volume in the SHH-activated subtype when compared to

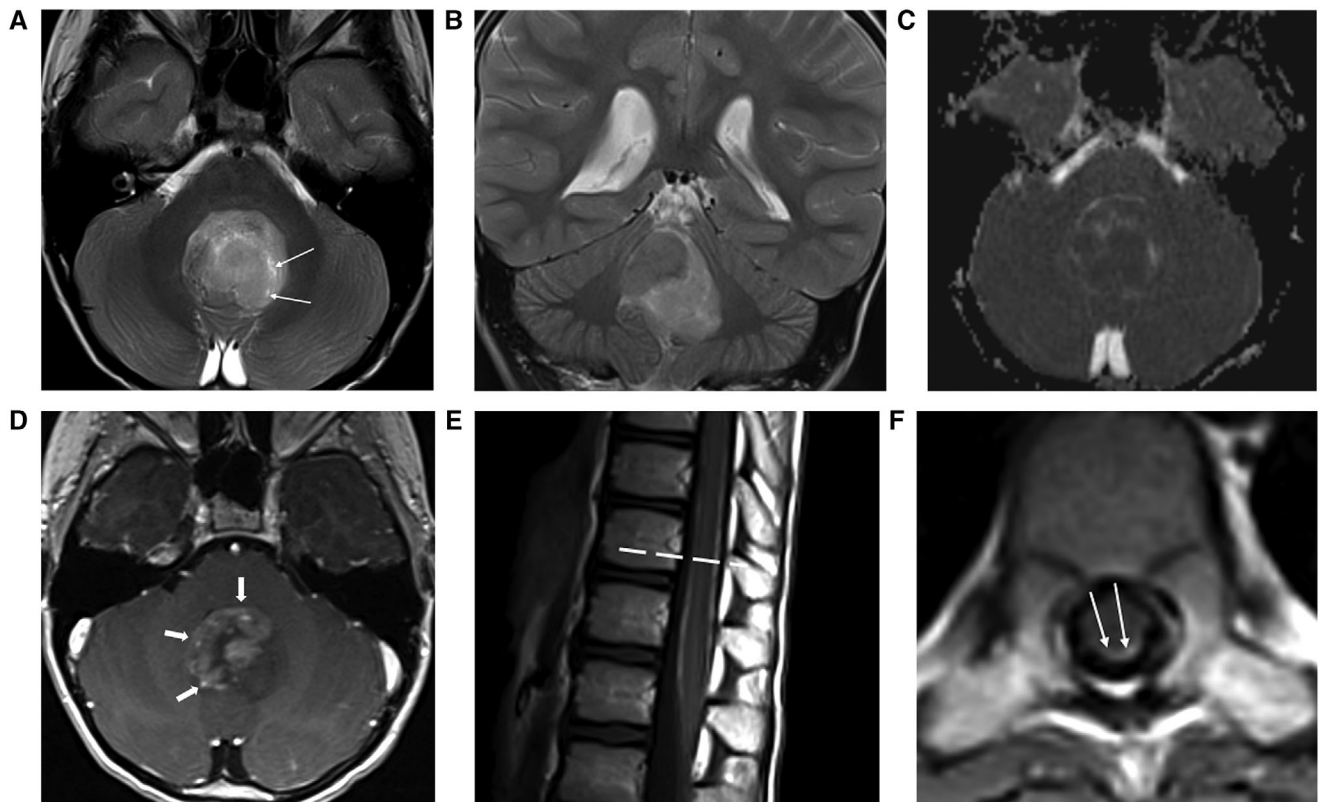


Fig 5. Non-Wingless/non-sonic hedgehog medulloblastoma (patient #29): Neuropathological tumor characteristics were a classic subtype in histopathology, a TP53 wild type, and a Ki67 of 40%. T2-weighted imaging showed a midline/cerebellar vermian tumor location with a volume of 17.9 cm³ and tiny intratumoral cysts (white arrows, A). Tumoral edema and hemorrhage were absent. No cerebrospinal fluid diapedesis was seen (B). Apparent diffusion coefficient (ADC) map with a calculated mean ADC (10^{-6} mm²/s) of 510 ± 46 standard deviation (C). Contrast-enhanced T1-weighted imaging (CET1WI) showed heterogeneous moderate contrast enhancement of the solid tumor (white bold arrows, D). CET1WI of the spine depicted leptomeningeal seeding (example level Th11, E; white slim arrows, F).

non-WNT/non-SHH group 4 medulloblastoma, and Perreault and colleagues.¹² On the other hand, five of 13 (38.5%) SHH-activated tumors of our study yielded no peritumoral edema, resulting in a relatively low sensitivity of 61.5%.

Univariate analysis did not reveal any statistically significant difference between genetic subtypes regarding several further conventional MRI parameters assessed in this study. In particular, differentiation of genetic subtypes was neither possible regarding the parameter hemorrhage (according to Keil and colleagues a prerequisite for non-WNT/non-SHH group 4 medulloblastoma¹¹) nor contrast enhancement (Perreault and colleagues suggested a predominantly minor contrast enhancement in non-WNT/non-SHH group 4 medulloblastoma¹²). However, each of the three WNT-activated medulloblastomas in the present study harbored at least small cysts but showed neither peritumoral edema nor MRI signs of metastatic disease (similar to the findings of Keil and colleagues¹¹), enabling differentiation to the SHH-activated subtype with a sensitivity and negative predictive value of 100%, each, in the multivariate testing. Thus, particularly the absence of metastatic disease at the time of initial diagnosis underlines the relatively benign biology of the WNT-activated subtype.⁶ According to our data, MRI-based differentiation between WNT-activated and non-WNT/non-SHH subtypes was not reliable, as both genetic subtypes were commonly located in the midline and showed no peritumoral edema. However, 50% of non-WNT/non-SHH tumors showed MRI signs of metastatic disease, even though this

difference was not statistically significant. Midline tumors were associated with obstructive hydrocephalus, as they showed a significantly larger volume than hemispheric or CPA medulloblastomas. But, in contrast to other authors,¹¹ the tumor volume was not significantly different between the genetic subtypes.

A major goal of the present study was to assess potential associations between the genetic subtypes and immunohistochemical parameters of medulloblastoma using quantitative (ADC) MRI, as comparable literature data are sparse. Considering the whole study population ($n = 32$), the calculated ADC_{mean} within the solid tumor components was 586 (10^{-6} mm²/s), which is in the range of data reported by other authors who did not explicitly investigate genetic subtypes.^{13,20,22} Similar to the results of Perreault and colleagues,¹² difference of the ADC_{mean} between genetic subtypes did not reach statistical significance, which was possibly caused by the low sample size of the WNT-activated subgroup ($P = .080$). However, the mean ADC value was lowest in this subgroup (480 [10^{-6} mm²/s]); this finding is comparable to recently published data of Reddy and colleagues.²⁹ They reported the same distribution of ADC values between genetic subtypes, with the lowest and highest ADC values within the solid tumor components of WNT-activated (594 [10^{-6} mm²/s]) and non-WNT/non-SHH subtypes (719 [10^{-6} mm²/s]), respectively.²⁹ Comparison of the ADC_{mean} between the histopathological subtypes of medulloblastoma yielded a significant difference between the desmoplastic and extensive

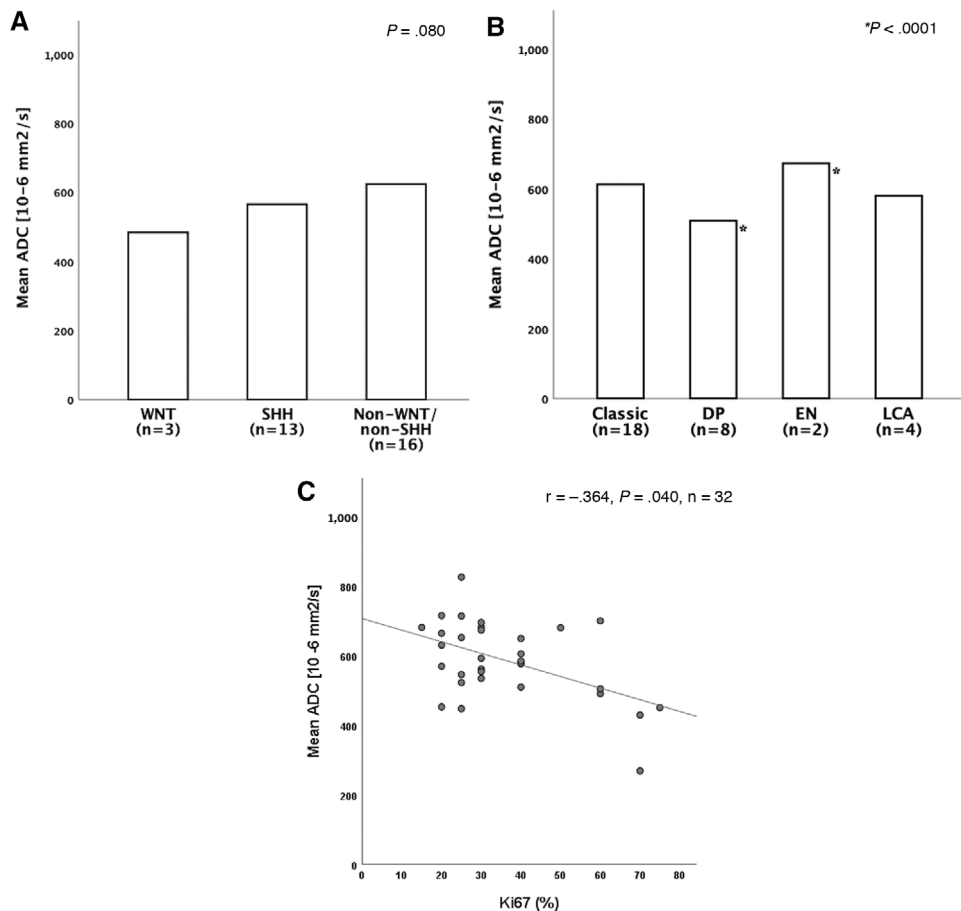


Fig 6. Quantitative analysis of mean apparent diffusion coefficient (ADC) values. Comparison of the mean ADC between genetic subtypes did not yield significant differences ($P = .080$; A). Regarding histopathology, the calculated mean ADC was significantly lower in desmoplastic subtypes when compared with medulloblastomas characterized by extensive nodularity (509 vs. 673 [10^{-6} mm²/s], $P < .0001$; *, B). A significant negative correlation was found between mean ADC and the proliferation index Ki67 ($r = -.364$, $P = .040$, $n = 32$; C). ADC = apparent diffusion coefficient; DP = desmoplastic; EN = extensive nodularity; LCA = large cell/anaplastic; n = number of patients; SHH = sonic hedgehog pathway activation; WNT = wingless pathway activation.

nodular subtype (509 vs. 673 [10^{-6} mm²/s]), even though this finding has to be interpreted with caution due to the low sample size of the latter group. In contrast, Yeom and colleagues¹³ reported a significantly lower ADC_{mean} in classic versus large cell/anaplastic medulloblastoma. In our study, SHH-activated medulloblastomas were associated with a desmoplastic, and both WNT-activated and non-WNT/non-SHH medulloblastomas with a classic histopathological subtype, which is congruent to previously published neuropathological data.^{4,30}

It is still unclear whether the immunohistochemical parameters in medulloblastoma patients may affect the ADC value within the solid tumor components as mentioned above. In this study, we found a significant negative correlation between ADC_{mean} and Ki67, contradicting the findings of other authors.¹⁰ Our data suggest that a low ADC value (ie, high cellular density) within the solid tumor may be associated with an increased proliferation rate. Moreover, the ADC_{mean} was statistically similar when comparing both TP53 wild type with aggressive TP53-mutated and nonmetastatic with metastatic medulloblastoma. We therefore believe that the ADC value does not necessarily reflect the tumor malignancy. This hypothesis is underlined by the relatively low ADC_{mean} in WNT-activated medulloblastoma calculated in this study

when compared to the more malignant subtypes (even though not statistically significant).

The results of the present study serve as hypothesis-generating only as they have to be evaluated in light of several limitations. A major drawback is the limited sample size particularly of WNT-activated tumors ($n = 3/32$, 9.4%) which clearly reflects the low overall incidence of this subtype. Furthermore, detailed non-WNT/non-SHH subtype information (group 3 or 4) is missing due to the retrospective study design. Finally, the ADC_{mean} was significantly lower in the 3 Tesla group (494 [10^{-6} mm²/s]) when compared to the 1.5 Tesla group (603 [10^{-6} mm²/s]; $P = .04$). However, control ADC measurements in healthy regions (gray and white matter, pure CSF) yielded no significant differences between magnetic field strengths. Thus, we believe that this difference was probably attributed due to the tumor itself. This hypothesis is underlined by the fact that the parameter “patient age” as a potential additional bias was also not associated with ADC values in normal appearing central nervous regions. We analyzed this parameter due to the wide age range (1-57 years) in our study population.

In conclusion, peritumoral edema was exclusively present in the aggressive SHH-activated subtypes and therefore the

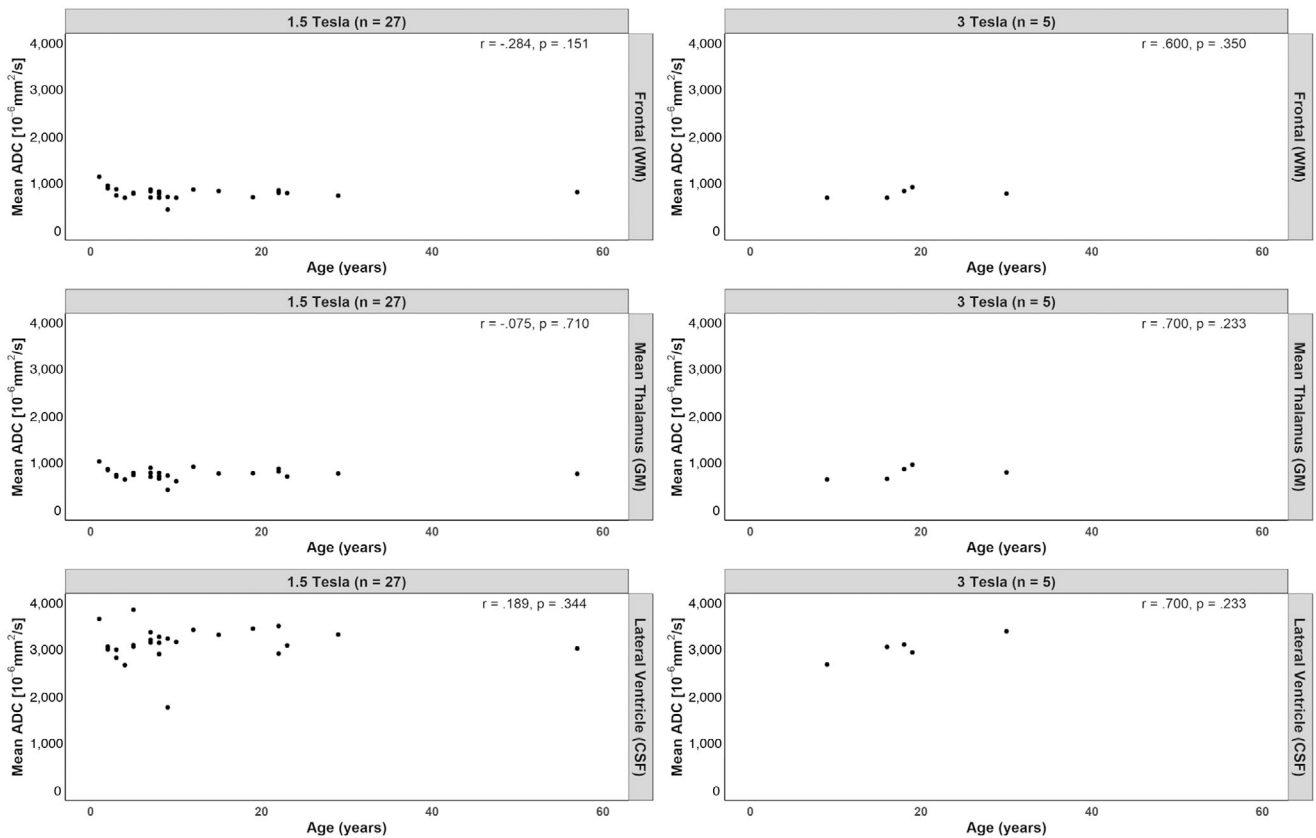


Fig 7. Relationship between mean apparent diffusion coefficient (ADC) values in selected healthy appearing central nervous regions and age with regard to the field strength of the MRI scanners. No significant correlations between ADC values and age were found. ADC values of the corresponding regions of interest were not significantly different between the field strengths. ADC = apparent diffusion coefficient; GM = gray matter; n = number of patients; WM = white matter.

most valuable MRI parameter to distinguish this entity from the other genetic subtypes. A hemispherical location was also strongly associated with SHH activation. Thus, presence of these two MRI parameters may yield a quicker initiation of SHH-targeted therapy regimens even before tumor resection. Differentiation between WNT-activated and non-WNT/non-SHH medulloblastoma was not suitable using MRI parameters, as both entities (among further imaging parameters) were commonly located in the midline and yielded no peritumoral edema. Albeit, none of the WNT-activated tumors showed signs of metastatic disease. ADC measurement alone was not reliable for genetic characterization of medulloblastoma, possibly caused by the low sample size of WNT-activated tumors. However, we found a trend toward lower and higher mean ADC values within solid tumor components of WNT-activated and non-WNT/non-SHH medulloblastoma, respectively. Furthermore, a low ADC value was associated with an increased proliferation rate. We recommend further ideally prospective multicenter studies with larger patient cohorts (particularly WNT-activated subtype) implementing follow-up MRI data, for example, to investigate the suggested MRI parameters in recurrent medulloblastoma.

References

- Partap S, Curran EK, Propp JM, et al. Medulloblastoma incidence has not changed over time: a CBTRUS study. *J Pediatr Hematol Oncol* 2009;31:970-1.
- Menyhárt O, Győrffy B. Molecular stratifications, biomarker candidates and new therapeutic options in current medulloblastoma treatment approaches. *Cancer Metastasis Rev* 2020;39:211-33.
- Louis DN, Perry A, Reifenberger G, et al. The 2016 World Health Organization classification of tumors of the central nervous system: a summary. *Acta Neuropathol* 2016;131:803-20.
- Pickles JC, Hawkins C, Pietsch T, et al. CNS embryonal tumours: WHO 2016 and beyond. *Neuropathol Appl Neurobiol* 2018;44:151-62.
- Zhukova N, Ramaswamy V, Remke M, et al. Subgroup-specific prognostic implications of TP53 mutation in medulloblastoma. *J Clin Oncol* 2013;31:2927-35.
- Robinson GW. Impact of tumor location on medulloblastoma subtyping and treatment. *Pediatr Blood Cancer* 2013;60:1393-4.
- Gajjar A, Chintagumpala M, Ashley D, et al. Risk-adapted craniospinal radiotherapy followed by high-dose chemotherapy and stem-cell rescue in children with newly diagnosed medulloblastoma (St Jude Medulloblastoma-96): long-term results from a prospective, multicentre trial. *Lancet Oncol* 2006;7:813-20.
- Ellison DW, Onilude OE, Lindsey JC, et al. β -catenin status predicts a favorable outcome in childhood medulloblastoma: the United Kingdom Children's Cancer Study Group Brain Tumour Committee. *J Clin Oncol* 2005;23:7951-7.
- Pietsch T, Haberler C. Update on the integrated histopathological and genetic classification of medulloblastoma: a practical diagnostic guideline. *Clin Neuropathol* 2016;35:344-52.
- Schob S, Beeskov A, Dieckow J, et al. Diffusion profiling of tumor volumes using a histogram approach can predict proliferation and further microarchitectural features in medulloblastoma. *Childs Nerv Syst* 2018;34:1651-6.

11. Keil VC, Warmuth-Metz M, Reh C, et al. Imaging biomarkers for adult medulloblastomas: genetic entities may be identified by their MR imaging radiophenotype. *AJNR Am J Neuroradiol* 2017;38:1892-8.
12. Perreault S, Ramaswamy V, Achrol AS, et al. MRI surrogates for molecular subgroups of medulloblastoma. *Am J Neuroradiol* 2014;35:1263-9.
13. Yeom KW, Mobley BC, Lober RM, et al. Distinctive MRI features of pediatric medulloblastoma subtypes. *Am J Roentgenol* 2013;200:895-903.
14. Wefers AK, Warmuth-Metz M, Pöschl J, et al. Subgroup-specific localization of human medulloblastoma based on pre-operative MRI. *Acta Neuropathol* 2014;127:931-3.
15. Teo WY, Shen J, Su JM, et al. Implications of tumor location on subtypes of medulloblastoma. *Pediatr Blood Cancer* 2013;60:1408-10.
16. Belli G, Busoni S, Ciccarone A, et al. Quality assurance multicenter comparison of different MR scanners for quantitative diffusion-weighted imaging. *J Magn Reson Imaging* 2016;43:213-9.
17. Grech-Sollars M, Hales PW, Miyazaki K, et al. Multi-centre reproducibility of diffusion MRI parameters for clinical sequences in the brain. *NMR Biomed* 2015;28:468-85.
18. Ogura A, Tamura T, Ozaki M, et al. Apparent diffusion coefficient value is not dependent on magnetic resonance systems and field strength under fixed imaging parameters in brain. *J Comput Assist Tomogr* 2015;39:760-5.
19. Koral K, Mathis D, Gimi B, et al. Common pediatric cerebellar tumors: correlation between cell densities and apparent diffusion coefficient metrics. *Radiology* 2013;268:532-7.
20. Payabvash S, Tihan T, Cha S. Differentiation of cerebellar hemisphere tumors: combining apparent diffusion coefficient histogram analysis and structural MRI features. *J Neuroimaging* 2018;28:656-65.
21. Wang W, Cheng J, Zhang Y, et al. Use of apparent diffusion coefficient histogram in differentiating between medulloblastoma and pilocytic astrocytoma in children. *Med Sci Monit* 2018;24:6107-12.
22. Takayasu T, Yamasaki F, Akiyama Y, et al. Advantages of high b-value diffusion-weighted imaging for preoperative differential diagnosis between embryonal and ependymal tumors at 3 T MRI. *Eur J Radiol* 2018;101:136-43.
23. Koral K, Alford R, Choudhury N, et al. Applicability of apparent diffusion coefficient ratios in preoperative diagnosis of common pediatric cerebellar tumors across two institutions. *Neuroradiology* 2014;56:781-8.
24. Pierce TT, Provenzale JM. Evaluation of apparent diffusion coefficient thresholds for diagnosis of medulloblastoma using diffusion-weighted imaging. *Neuroradiol J* 2014;27:63-74.
25. Albert FK, Forsting M, Sartor K, et al. Early postoperative magnetic resonance imaging after resection of malignant glioma: objective evaluation of residual tumor and its influence on regrowth and prognosis. *Neurosurgery* 1994;34:45-60.
26. Chang CH, Housepian EM, Herbert C. An operative staging system and a megavoltage radiotherapeutic technic for cerebellar medulloblastomas. *Radiology* 1969;93:1351-9.
27. Poretti A, Meoded A, Cohen KJ, et al. Apparent diffusion coefficient of pediatric cerebellar tumors: a biomarker of tumor grade? *Pediatr Blood Cancer* 2013;60:2036-41.
28. Patay Z, DeSain LA, Hwang SN, et al. MR Imaging characteristics of Wingless-Type-subgroup pediatric medulloblastoma. *AJNR Am J Neuroradiol* 2015;36:2386-93.
29. Reddy N, Ellison DW, Soares BP, et al. Pediatric posterior fossa medulloblastoma: the role of diffusion imaging in identifying molecular groups. *J Neuroimaging* 2020;30:503-11.
30. Kool M, Korshunov A, Remke M, et al. Molecular subgroups of medulloblastoma: an international meta-analysis of transcriptome, genetic aberrations, and clinical data of WNT, SHH, Group 3, and Group 4 medulloblastomas. *Acta Neuropathol* 2012;123:473-84.